In vitro study of bioactive glass coatings obtained by atmospheric plasma spraying

Eugeni Cañas [a],*, Alina Grünewald [b], Rainer Detsch [b], María José Orts [a], Enrique Sánchez [a], Aldo R. Boccaccini [b],*

[a] Instituto de Tecnología Cerámica (ITC), Universitat Jaume I (UJI), Castellón, Spain
[b] Institute of Biomaterials, University of Erlangen – Nuremberg, Erlangen, Germany

ABSTRACT

This research has addressed a complete study of the bioactivity of bioactive glass coatings obtained by atmospheric plasma spraying. The coatings have been characterized in terms of microstructure, adhesion, crystalline phases and bioactivity. Hydroxycarbonate apatite formation was also monitored following a standard protocol and the in vitro cell response was evaluated by human osteoblast-like cells (MG-63 cells) incubation.

The obtained coatings shown a microstructure typical of glass coatings. A simulated body fluid test proved that coatings are capable of developing a surface layer of hydroxycarbonate apatite whereas the appearance of this phase takes place at a longer time than that observed for the powder feedstock. Cell-culture test showed multidirectional growth of MG-63 cells which promoted good contact between cells and the surface of the coating. This study has confirmed a positive effect of the coatings in terms of surface bioactivity and, more interestingly, it has proven an adequate cell-material interaction on the coating surface.

© 2020 SECV. Published by Elsevier España, S.L.U. This is an open access article under the CC BY-NC-ND license (http://creativecommons.org/licenses/by-nc-nd/4.0/).

Estudio in vitro de recubrimientos de vidrio bioactivo depositados mediante proyección térmica por plasma atmosférico

RESUMEN

Este trabajo ha abordado un estudio completo de la bioactividad de recubrimientos de vidrio bioactivo depositados mediante proyección térmica por plasma atmosférico. Se han caracterizado la microestructura, la adherencia, las fases cristalinas y la bioactividad de los recubrimientos obtenidos. También se ha estudiado la formación de hidroxiapatita carbonatada siguiendo un protocolo estándar y se ha evaluado la respuesta in vitro de los recubrimientos mediante su incubación con osteoblastos humanos (células MG-63).

* Corresponding authors.
E-mail addresses: eugeni.canas@itc.uji.es (E. Cañas), aldo.boccaccini@fau.de (A.R. Boccaccini).

Los recubrimientos obtenidos han mostrado una microestructura típica de recubrimientos de vidrio. Tras la inmersión en fluido biológico simulado, se ha comprobado que el recubrimiento es capaz de desarrollar una capa superficial de hidroxiapatita carbonatada, aunque la velocidad de aparición de esta capa es menor que la observada para el polvo de vidrio de partida. El ensayo de cultivo celular ha mostrado un crecimiento multidireccional de las células MG-63, dando lugar a un buen contacto entre las células y la superficie del recubrimiento. Este estudio ha confirmado un efecto positivo de los recubrimientos en términos de bioactividad de la superficie y, lo que es más interesante, ha demostrado una adecuada interacción célula-material sobre la superficie del recubrimiento.

Introduction

Atmospheric Plasma Spraying (APS) is a highly employed technique to produce coatings from powder feedstocks for a wide range of applications, such as biological coatings from hydroxyapatite feedstocks [1]. Moreover, with the development of bioactive glasses (BGs), this technique has also become promising for obtaining coatings from this type of materials [1–3]. The reasons for this growing interest in such coatings are: (i) the glass coatings obtained preserve the amorphous structure that gives rise to a higher bioactivity than that of hydroxyapatite, without the need for any treatment after deposition, (ii) easier control of coatings' morphology, thickness and structure, and hence of coatings' properties [1].

Thus, literature shows numerous recent works where thermal spray conditions have been optimized in order to obtain coatings with good mechanical (adhesion to the substrate) and functional properties (bioactivity). Many of these works use the Bioglass® composition developed by Hench et al. commonly called 45S5 [4,5]. However, other compositions derived from 45S5 Bioglass® have also been developed in order to modify the melting ability of the glass during thermal spraying or the final bioactivity of the glass coating [6–9].

Early studies on plasma sprayed BG coatings used glass powder obtained by means of the conventional technique of "melting and crushing". It has been shown that the projection was subordinated to the fluidity of the powder feedstock employed, which limited the possibility of feeding micron-sized powders of poor flowability [10]. For this reason, recent research was carried out using glass powder suspensions as plasma feedstock, which correspond to the technique known as Suspension Plasma Spraying (SPS) [11,12]. In this case, it is possible to use glass powder with a micron or even submicron particle size, although suspensions of non-aqueous nature must be used for this purpose to avoid glass leaching [13]. The use of liquid precursors of bioactive glass known as the Solution Precursor Plasma Spraying (SPPS) technique is a much more recent development [14]. Although the preparation of bioactive glasses by the sol–gel technique is quite common, the use of colloidal precursors in plasma spraying is a very recent approach [15–17]. This thermal spraying technique is especially interesting because it greatly simplifies the feedstock preparation process, as the preparation of the glass powder is not necessary, with the consequent savings of time and energy and increment of feedstock purity. Recently published results are promising regarding the microstructure and properties of the BG coatings obtained [18,19].

Previous research efforts have focused on the optimization of the feedstock characteristics, either solid or liquid, as well as on the spraying conditions in order to design an adequate microstructure in the final coating that allows coatings with a good adherence to the substrate as well as high bioactivity to be obtained. Although results are promising, BG coatings suffer poor adhesion while the bioactivity is quite acceptable. However, the determination of bioactivity has been carried out, in most cases only by means of simulated body fluid (SBF) tests [2,11,20,21], monitoring the formation of hydroxyapatite on the surface. Although a SBF test represents a simple and quick way of assessing coating bioactivity, a more completed in vitro characterization is necessary to address the ability of the coating to form bone tissues. To the best of our knowledge, very few works about cell tests on plasma-sprayed bioactive glass coatings have been performed [22–24]. Therefore, the capacity of cell-material response of this type of coatings as well as the relationship between coating microstructure and biological response are still scarcely understood.

From the foregoing, it is concluded that there is a need to carry out a more thorough evaluation of the cell biology response to bioactive glass coatings obtained by plasma spraying. Hence, this research has been carried out with the aim of: (i) developing and characterizing a bioactive glass coating by atmospheric plasma spraying from glass powder with an adequate microstructure and adherence to the substrate; (ii) determining and monitoring its bioactivity over time by means of in vitro SBF and cell culture tests; and (iii) relating the biological response results with the microstructural characteristics of the resulting coating.

Experimental

Bioactive glass powder feedstock preparation

A powder feedstock of 45S5 bioactive glass referred as BG sample was prepared by melting a mixture of analytical grade SiO_2, Ca_3PO_4, $NaCO_3$ and $CaCO_3$ in a home-made rotatory furnace as shown in previous works [10]. The resulting melt was then quenched in water obtaining the frit. The chemical composition of the frit determined by wavelength dispersive X-ray fluorescence spectrometry (AXIOS, PANalytical, Netherlands) was (in wt%): 47.6 SiO_2, 5.3 P_2O_5, 23.1 CaO and 24.0 Na_2O which

Table 1 – Plasma spray conditions used to spray the coating.

Spraying parameters	Bioactive glass coatings
Ar (slpm)[a]	25–38
H$_2$ (slpm)[a]	15
Intensity (A)	600
Spraying distance (m)	0.11
Torch scan velocity (m s^{-1})	1.00
Powder mass flow (kg s^{-1}) $\times 10^3$	0.25
Nozzle diameter (m) $\times 10^3$	2.00

[a] Standard liter per minute.

is very close to the nominal 45S5 BG composition. The frit was subsequently processed according to the following steps: dry grinding in a hammer mill and sieving the resulting material to obtain a powder with a maximum particle size of 63 μm. Fig. S1 of the Appendix/Supplementary information displays the morphology and the phase nature of the particles.

In order to enhance flowability of the glass powder feedstock, a hydrophobic fumed silica-based fluidiser (Aerosil R812, Evonik Industries, Germany) was added to the powder as previously reported [10]. The fluidiser was mixed with the fine powder by means of a high-intensity knife-type mixer. This fluidiser can be observed in the previous work [10], partially coating the glass particles.

Bioactive glass coatings deposition and characterization

The next step was the deposition of the bioactive glass powder by Atmospheric Plasma Spraying (APS). In order to do so, a thermal spraying facility was used, whose details are reported in [10]. The spraying conditions employed are listed in Table 1. Two different flow rates of argon were used; 25 slpm (standard liter per minute) (BGC25 experiment) and 38 slpm (BGC38 experiment). Comparing both conditions, the mixture with 25 slpm argon is more energetic than the other one, as hydrogen is less diluted and consequently, after the ionization of the mixture, the plasma plume released possesses a higher enthalpy and, henceforth, a greater melting capacity for the particles [25]. Contrariwise, the mixture of 38 slpm argon gives a higher momentum to the injected particles (particles at impact get more splashed) than the other mixture as both argon and total gas flow rates are greater. Moreover, the higher momentum results in less residence time of the particles inside the plasma plume and hence they arrive at the substrate less molten. AISI type 304 stainless steel disks with 0.025 m of diameter were used as substrates. Before the deposition of the coatings, the substrates were grit-blasted with black corundum and cleaned with ethanol, as reported in a previous work [10]. Only one face of the substrates was prepared and hence coated.

The microstructure of the obtained coatings was observed in a field-emission gun environmental scanning electron microscope (FEG-ESEM) (QUANTA 200FEG, FEI Company, USA) using the backscattering electron detector signal under high vacuum conditions. Coating thickness and porosity were estimated by image analysis (MicroImage) at 2000x magnifications from FEG-ESEM pictures. 20 FEG-ESEM images were examined, and the findings averaged. Moreover, the nature of the

coatings (amorphous or crystalline) was determined by X-ray diffraction (XRD; Advance diffractometer, Bruker Theta-theta, Germany). The XRD analysis was done using Cu Kα radiation at a working power of 30 kV and 40 mA. In addition, a range of 2θ between 10° and 80° was employed, with a step size of 0.02° and a scanning speed of 0.5 s step^{-1}. Finally, the adhesion strength was determined by the pull-off method known as tensile adhesion test (TAT) following the ASTM-C633 standard. For this examination, 3 samples of each coating were tested using a universal testing machine (Instron 5889, Instron, UK). The test was carried out at a constant rate of cross-head travel of 1.7×10^{-5} m s^{-1}, recording the tensile load at which the rupture of the coating occurred (maximum tensile load). From the recorded load, the adhesion of the coatings was determined, and the obtained results were averaged.

SBF tests

The bioreactivity of both the powder developed and the coatings was studied by immersing them in Simulated Body Fluid (SBF) following a standard protocol [26]. First, SBF was prepared following the method of Kokubo [27], and then the powders and coatings were soaked in SBF inside plastic vessels.

For the powders, a ratio of 1.5 kg of powder per m^3 of SBF was used. The vessels containing the powders were incubated inside a water bath at 36.5 ± 0.5 °C during 1 h and 1, 2, 5 and 7 days. For each soaking time, 3 different aliquots of powder were used.

In the case of the coatings, the amount of SBF needed was calculated using the following relation:

$$V_{SBF} = \frac{S_C}{10} \tag{1}$$

where V_{SBF} is the volume in m^3 of SBF and S_C is the area in m^2 of the sample (glass coating). As said before, substrates of 0.025 m diameter were used, corresponding to a face area of 4.9×10^{-4} m^2, and hence 4.9×10^{-5} m^3 of SBF were used for each coating sample. The vessels containing the coated discs were incubated inside a water bath at 36.5 ± 0.5 °C during 1, 2, 5, 7 and 14 days. For each soaking time, 3 different coated discs were used, which were placed inside the vessel perpendicular to the bottom part.

Regardless of the type of sample (powder or coating), after each soaking time the pH of the SBF was measured. For comparison purposes, vessels filled with only SBF were incubated inside the water bath at 36.5 ± 0.5 °C during 1, 2, 5, 7 and 14 days as a control, and after each time the pH was also measured. Then, the sample object of study (powder and coating) was removed from the vessel, gently rinsed with distilled water and its surface morphology was observed by FEG-ESEM. In addition, the nucleation and growth of the hydroxycarbonate apatite (HCA) was followed by Fourier transform infrared spectroscopy (FTIR) (Nicolet 6700, Thermo Scientific, USA), energy-dispersive X-ray microanalysis (EDX) (Genesis 7000 SUTW, EDAX, USA) and XRD. The samples for FEG-ESEM, were carbon coated by sputtering before inspection and the observation was done using the secondary electron detector signal under high vacuum conditions. FTIR was performed

in absorbance mode, with a spectral resolution of $2\,cm^{-1}$ from 1500 to $500\,cm^{-1}$. EDX analysis was done at the same conditions as the FEG-ESEM observation and XRD using the parameters set out in the previous section.

Cell culture

For the cell culture study, human osteoblasts-like cells (MG-63, Sigma–Aldrich, USA) were chosen and cultured in Dulbecco's modified eagle's culture medium (DMEM, Gibco, Germany) in humidified atmosphere of 5% CO_2 in air at 37 °C. The DMEM contained 10% fetal calf serum (FCS, Sigma–Aldrich, USA) and 1% antibiotics (containing penicillin + streptomycin). The culture medium was changed every 2–3 days.

The resulting coating from BGC25 experiment and uncoated AISI type 304 stainless steel were tested for the sake of comparison. Both type of samples (coated and uncoated) were cut into small squares with approximately $0.95 \times 10^{-2}\,m$ of side. Then, all samples were sterilized in electric furnace for 2 h at 160 °C and preincubated in DMEM at 37 °C in humidified atmosphere of 10% CO_2 in air for 48 h. The main purpose of the preincubation was to avoid a high pH increase of the cell culture medium after seeding the cells to prevent their death, especially in the case of the bioactive glass coated samples, a phenomenon that has been reported frequently in literature [28,29].

After that, cell culture medium (ccm) or DMEM was removed from the culture flask and cells were washed with phosphate-buffered saline solution (PBS, Gibco, Germany) and detached from the same with $3 \times 10^{-6}\,m^3$ of trypsin/EDTA (Gibco, Germany). Then, $9 \times 10^{-6}\,m^3$ of DMEM at 37 °C was added into the flask to inhibit the trypsin effect and a sample was taken to count the number of cells. Then, prewarmed ccm was used to dilute the cell suspension in order to achieve the desired amount of $5 \times 10^{1\circ}$ cells/m^3.

Thereafter, the samples were placed inside untreated well plates of $3.14 \times 10^{-4}\,m^2$ area and cells were seeded onto them. $1 \times 10^{-6}\,m^3$ of ccm containing cells was placed in each well. In addition, 9 wells without sample were seeded with DMEM containing cells as a control sample. Afterwards, the plates were incubated inside an incubator at 37 °C in a humidified atmosphere of 10% CO_2 in air for 24 h. Finally, cells distribution, adhesion and morphology were analyzed.

Cell adhesion and morphology

Phalloidin-staining was used for cell morphology and adhesion while Vibrant-staining was employed to count the number of cells on the samples.

For phalloiding-staining, first the ccm was removed and the samples were washed with PBS. Then, the cells were fixed to the samples with a fixing solution (FluoFix-PBS) for 15 min, washed again and permeabilized with a permeabilization buffer for 5 min. At that point, a fluorescein isothiocyanate solution (Phalloidin, Sigma–Aldrich, USA) was added to each well for detecting the cytoskeleton, and the plate was incubated for 1 h in dark. After washing again with PBS, a Dapi solution was prepared with a concentration of $1 \times 10^{-9}\,m^3$ of 4′,6-Diamidino-2-phenylindole, dihydrochloride (Dapi, Sigma–Aldrich, USA) per $1 \times 10^{-6}\,m^3$ of PBS and

added into the wells for 5 min for observing nuclei. Finally, samples were washed with PBS and preserved in fresh PBS in the dark. For each sample, pictures were taken using a fluorescence microscope (Axio Scope A1, Carl Zeiss, Germany) at 5× and 20× magnifications.

Concerning the Vybrant-staining, the procedure was very similar to that used in the previous staining. The ccm was removed and the well plates were washed with PBS. Next, a mastermix solution, containing $4 \times 10^{-9}\,m^3$ Dil cell solution (Vybrant, Thermo Fisher Scientific, USA) per $1 \times 10^{-6}\,m^3$ of ccm, was added to each well and the plates were incubated for 45 min at 37 °C. Then, the solution was removed, the plates were washed with PBS and a fixing solution was put in the wells for 15 min. After removing that solution, a Dapi solution was prepared again with a concentration of $1 \times 10^{-9}\,m^3$ of Dapi per $1 \times 10^{-6}\,m^3$ of PBS and added into the wells for 5 min. Finally, samples were washed with PBS and preserved in fresh PBS in the dark. For cell counting with Vybrant-staining, 6 bioactive glass coated samples, 6 AISI type 304 stainless steel samples and 6 wells without samples were used. For each sample, 5 micrographs at 10× magnification were taken with fluorescent microscope and the number of cells was counted with ImageJ software. The results obtained from viable cells were also evaluated by one-way analysis of variance (ANOVA) with Tukey test with a significance statistical level of 0.01, in order to assess the statistical significance of the results [28,30].

Scanning electron microscope examination

The samples which were not used for the staining, were examined by scanning electron microscopy. After 24 h of incubation, ccm was removed from the wells and the samples were gently rinsed with PBS. Then, after adding two different fixing solutions (the first one containing glutaraldehyde + sodium cacodylate and the second one containing glutaraldehyde + sodium cacodylate + paraformaldehyde) for 1 hour each, the samples were dehydrated with an ethanol series starting from a concentration of 30% until 100%. Finally, the samples were put inside a critical point dryer, and after that they were carbon coated and observed by FEG-ESEM.

Results and discussion

Coatings characterization

Surface and cross-section micrographs of the obtained coatings are displayed in Fig. 1. Typical APS coatings obtained from highly refractory crystalline ceramic oxides such as alumina or zirconia, result in microstructures composed of completely flatten splats. However, the obtained coatings in the present work exhibit a microstructure comprising partially deformed splats, and plenty of typically rounded pores from trapped gas as reported in previous investigations on plasma sprayed glass coatings [7,11,12,31]. This microstructure is associated to the melting behavior of glass particles during the plasma deposition process, which is mainly influenced by the energy of the plasma plume. In both experiments, the particles achieved a semi-molten state with a rounded shape composed of an unmelted core surrounded by a molten glass layer. When these
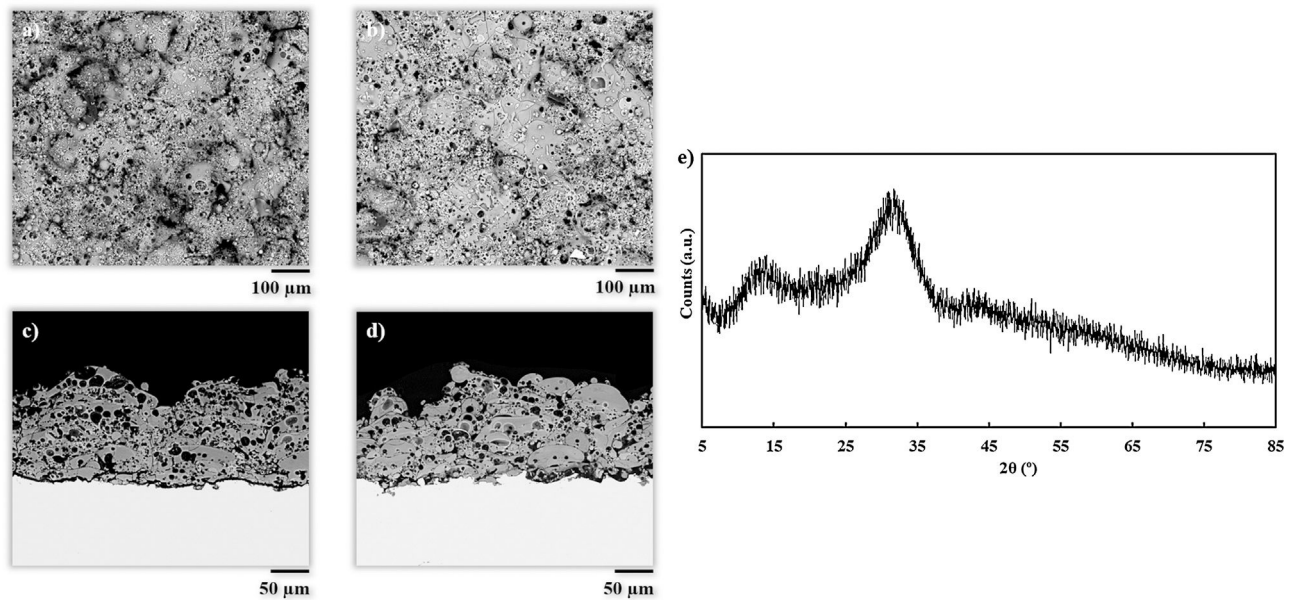
Fig. 1 – FEG-ESEM micrographs of the obtained coatings: (a) surface and c) cross-section for the coating deposited with 38 slpm of argon, (b) surface and (d) cross-section for the coating deposited with 25 slpm of argon, (e) XRD pattern of the 25 slpm argon deposited coating.

rounded particles impact onto the substrate, they remain attached to it due to this molten glass layer, but their flattening is prevented by the un-melted core. As it can be observed in Fig. 1, this effect is more visible to BGC38 coating (Fig. 1a and c) where a higher flow rate of argon was used. Therefore, as mentioned above, two effects took place simultaneously inside the plasma plume, that is hydrogen is more diluted resulting in a lower thermal conductivity through the plasma plume and lower residence time of the particle inside the plume. In contrast, for BGC25 coating, the higher thermal conductivity of the plasma plume combined with the higher residence time of the particles inside the plume, resulted in a thicker glass molten layer surrounding the core of the particles, giving rise to more flattened splats. These findings confirm previous results reported in the literature by Canillo et al. [31]. According to these researchers, from the observation of these heterogeneous microstructures, low values of adhesion strength can be expected. Nevertheless, the rough surface of the coatings and their porosity could exert a positive influence, enhancing the bioactivity and osteoconductivity of the resulting coating [32,33].

Table 2 shows some characteristics of the obtained coatings and their comparison with typical data for standard plasma spray coatings: deposition efficiency, thickness, porosity and adhesion strength [34,35]. Porosity for both coatings is higher than that observed to APS coatings as commented above. In addition, the differences in porosity between both coatings are also related to the microstructure. In fact, from Fig. 1 it can be appreciated that in the case of the BGC38 coating, the predominant type of pore is not rounded but with irregular, inter-splat shape due to the higher un-flattened state of this coating. As said above, due to the lower melting of the glass particles, the particle's core remains unmelted preventing the particle to be totally flattened when they impact onto the substrate or the as-deposited coating. Therefore, they compact worse among themselves when stacking on the substrate to develop the coating giving rise the irregular pores. The deposition efficiency of the BGC38 and BGC25 coatings are in agreement with typical data of APS coatings; however, the thicknesses are in the lower range compared to APS layers. Although much higher thickness can be easily obtained by increasing the number of plasma torch passages, this is probably of scarce interest

Table 2 – Some characteristics of the obtained coatings compared with typical standard APS coating data [34,35].

Characteristic	BGC25	BGC38	Standard APS coatings
Deposition efficiency (%)	90	83	90–95
Thickness (μm)	118.5 ± 4.5	100.0 ± 4.5	300–1500[a]
Porosity (%)	26.5 ± 3.0	33.0 ± 1.3	7–10[b]
Tensile adhesion strength (MPa)	4.4 ± 0.8	2.3 ± 1.0	15–25[c]

[a] Might be intentionally lower [34].
[b] Might be intentionally greater [34].
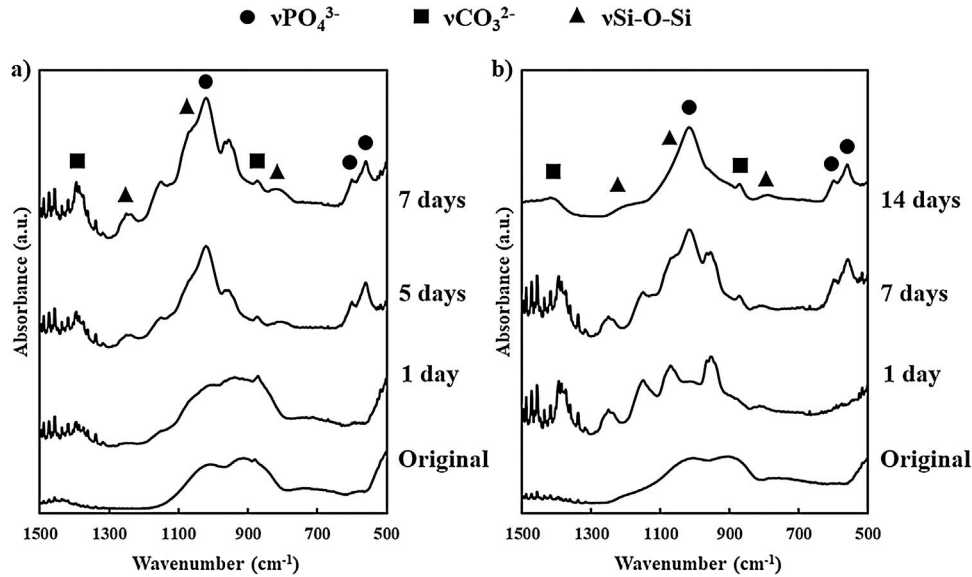[c] Ceramic coatings with bond coat.

Fig. 2 – FTIR results before and after soaking in SBF at different times: (a) for bioactive glass powder and (b) for BGC25 coating.
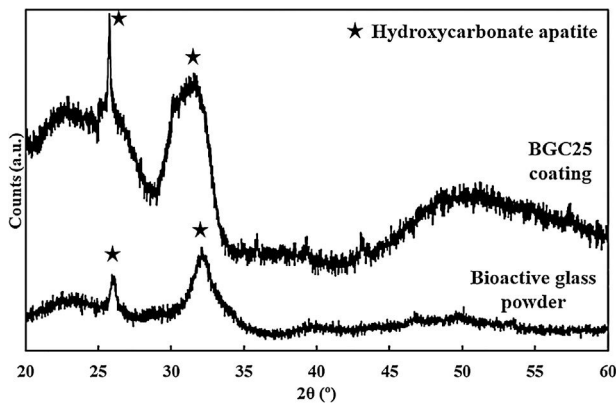

Fig. 3 – XRD patterns for the powder feedstock and the BGC25 coating samples after SBF immersion for 7 days and 14 days respectively.
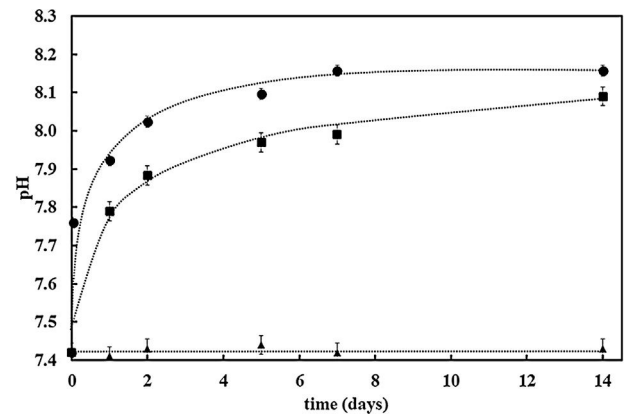

Fig. 4 – Evolution of SBF pH with immersion time for the bioactive glass powder (circle dots), the BGC25 coating (square dots) and SBF without any sample (triangle dots).

for biocoating application (100–150 μm maximum thickness) [1,36,37]. Again, the differences between the obtained coatings in both porosity and thickness are related to the melting state of the particles when impacting onto the substrate. Finally, regarding the adherence between the coatings and the substrate, lower adhesion values than some reported in the literature were obtained [38]. This fact could be due to using thinner substrates (1.00×10^{-2} m) than the stablished by the ASTM-C633 standard (3.81×10^{-2} m) [39]. Therefore, the substrates used in the present work are less ductile, causing a negative effect on the stress distribution inside the substrate during the tensile test. Even so, these values were found in good agreement with the other authors who tested similar probes [39]. Comparing both samples, the higher porosity of the BGC38 coating involves lower adhesion properties respect to the BGC25 coating. In any case, the final adhesion of the obtained coatings could be enhanced by using a common TiO_2 bond coat, which has been proven as an efficient way of significantly increasing this adhesive strength [38].

Fig. 1e shows the X-ray diffraction pattern of the BGC25 coating. As observed, the amorphous structure of the feedstocks (Fig. S1) was fully preserved. The XRD pattern of the other coating was very similar. As reported elsewhere, extremely high cooling rates occurring during plasma spraying prevent glass splats from recrystallisation, resulting in a fully amorphous layer [40]. This high cooling rate represents another great advantage of plasma spray technique to obtain bioactive glass coatings as glass devitrification can then be easily avoided. As reported in literature, the preservation of this amorphous structure seems to be a key issue in order to enhance the bioactivity response [41].

Powder and coating bioactivity by SBF test

SBF test of the samples was done to analyze the bioreactivity of the bioactive glass powder feedstock and coatings, but only the BGC25 coating was tested. Although both coatings were completely amorphous and presented similar surface roughness,
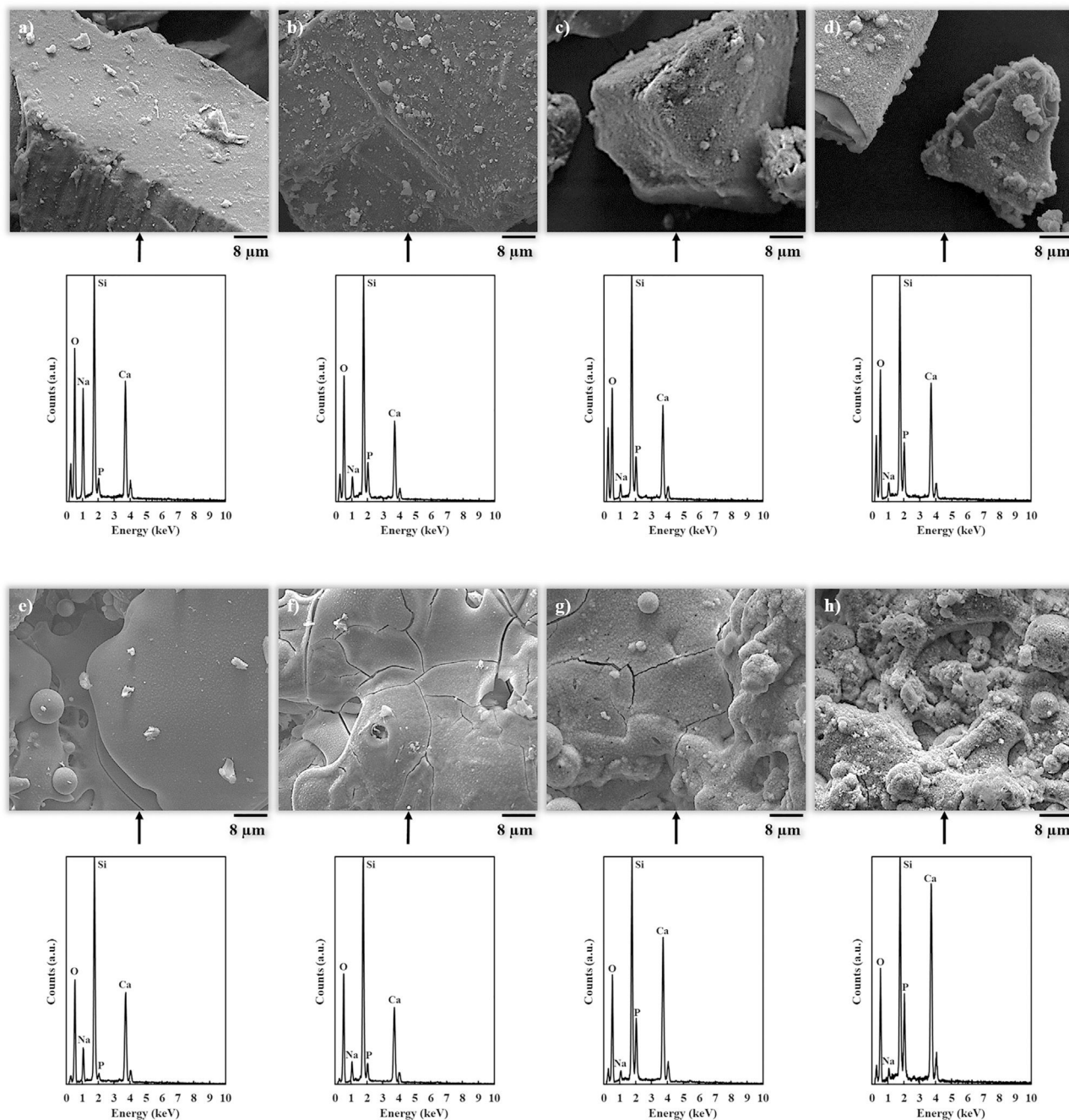
Fig. 5 – FEG-ESEM micrographs of the samples after different exposure time in SBF accompanied by their corresponding EDX analysis. From (a) to (d) bioactive glass powder before soaking and soaked for 1, 5 and 7 days, respectively. From (e) to (h) BGC25 coating before soaking and soaked for 1, 7 and 14 days, respectively.

the BGC38 coating was rejected as it had less thickness and adhesion to the substrate, as well as a higher closed porosity resulting in a less cohesive microstructure due to the spraying parameters, as described above.

FTIR results from BG powder and BGC25 coating before and after soaking in SBF are presented in Fig. 2. Before soaking both samples in SBF, they displayed similar spectra (since the composition is the same), exhibiting Si—O—Si stretching bands [42]. Nevertheless, as the samples were soaked and residence time inside SBF increases, the resulting FTIR spectra became different. Consequently, new absorption bands can be appreciated at $560\,cm^{-1}$ and $605\,cm^{-1}$, which correspond to P—O bending from PO_4^{3-} group, and at $1050\,cm^{-1}$ corresponding to P—O stretching [40,43]. Moreover, some bands at $800\,cm^{-1}$ (Si—O non-bonding oxygen), and $1070\,cm^{-1}$ and $1200\,cm^{-1}$ (Si—O—Si stretching) can be appreciated [42]. Additionally, bands at $870\,cm^{-1}$ and $1400\,cm^{-1}$, characteristic of CO_3^{2-} group, were also found, which are a clear sign of HCA formation mimicking bone like apatite since the formation of pure hydroxyapatite (HA) is unlikely in SBF [27].

Both types of samples display the same absorption bands. However, for the coating, the appearance of those bands takes place at a longer time than that observed for the bioactive glass powder feedstock. Absorption bands for the powder were fully evolved after 7 days in SBF while for the coating it took 14 days. This delay deals with the lower reactivity of the coating as a consequence of the sintering of the glass particles during plasma spraying at a high temperature. To confirm this result, the specific surface area of the powder feedstock and the coating were determined by BET (TriStar 3000, Micromeritics, The USA). For the BGC25 coating, due to its low adhesion, it was carefully detached [44,45], and then fragmented into pieces to carry out the measurement. The specific surface area was $4.70 \times 10^{-1} \, \text{m}^2/\text{g}$ for the powder and $6.35 \times 10^{-2} \, \text{m}^2/\text{g}$ for the coating, which clearly explains the lower reactivity (available surface) of the coating in comparison with the powder feedstock.

Although the bands detected for both the powder and the coatings correspond to the presence of HCA, XRD was also performed to corroborate the FTIR results and confirm the phase nature of the crystals developed [26,46]. The resulting patterns are shown in Fig. 3, where only the characteristic peaks of HCA at 2θ of 26° and 32° can be seen [27]. These peaks become sharper at 7 days and 14 days for the powder feedstock and the BGC25 coating, respectively.

Further confirmation of the impact of the surface reactivity on the kinetics of the HCA formation can be deduced when observing pH evolution during SBF test for both samples (bioactive glass powder and BGC25 coating) compared to the SBF without any sample. Fig. 4 shows the pH increase of SBF containing both samples (powder and coating) as the test progresses as a consequence of the chemical interaction occurring between SBF and the glass surface [27]. More remarkable, starting with an initial pH value of 7.42, bioactive glass powder shows a much faster pH increase during the first hours of immersion. As reported elsewhere, this first step in the SBF immersion test relates to cation (mainly Na$^+$ and Ca^{2+}) release from the glass which takes place more rapidly for the bioactive glass powder sample compared to the coating due to its higher exposed surface area [47].

FEG-ESEM images of the HCA layer developed onto the powder and coating surfaces at different soaking times are displayed in Fig. 5 followed by their corresponding EDX analysis spectrum. Powder micrographs (Fig. 5a–d) show that HCA formation starts to be noticeable after 1 day and fully developed after 7 days in SBF. For the coating (Fig. 5e–h), HCA formation is observed after 7 days, which develops further covering the surface after 14 days. For both the powder and the BGC25 coating, the EDX spectra presented in Fig. 5 confirms the appreciations from FEG-ESEM micrographs. P and Ca peaks grow as the immersion time increases, becoming fully developed after 7 days and 14 days exposure times for bioactive glass powder feedstock and BGC25 coating, respectively. Moreover, the intensity of the Na peak decreases as the soaking time increases confirming the cation exchange from the glass (powder or coating) to the SBF environment.
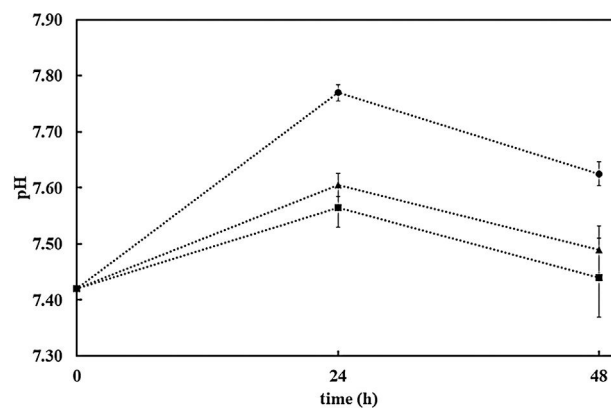
Fig. 6 – Medium pH variation during preincubation in 10% CO$_2$ humidified atmosphere. DMEM (square dots), AISI304 + DMEM (triangle dots) and BG25C + DMEM (circle dots).

Biological response

The resulting pH variation of the medium (DMEM) in the three cases set out above (without sample, with AISI304 uncoated sample and the BGC25 coating) is shown in Fig. 6. There is hardly any difference between the pH values of DMEM alone and that of AISI304 compared to the sample coated with BG. Thus, when releasing cations (Na$^+$ and Ca^{2+}) into the medium, the pH values always grew. However, after 48 h the pH of the medium is lower than 7.7 in all cases, which makes it possible to seed the cells on the samples and their subsequent incubation.

After incubation, the adhesion, distribution and morphology of the cells in direct contact with the samples were assessed according to the procedures described in the experimental section. In Fig. 7, the cells are shown after phalloidin-staining at different magnifications. The cells are identified by fluorescent coloration, the cytoskeleton cell being red and the nuclei blue. From these micrographs, it is possible to appreciate a large concentration of cells well adhered and scattered on the surfaces of both samples (AISI304 and BGC25 coating), which confirms their good biocompatibility. Nevertheless, different cell morphologies can be appreciated depending on the surface. The cells on the surface of the AISI304 substrate display an elongated rhomboid shape very similar to that of the control cells, while for the BGC25 coating the cells present a star-shaped morphology with higher number of cytoplasmic extensions (enhancing the contact between cells and cells-surface). This different morphology could be caused by both the surface topography (rough surface) and the ion release from the glass coating which promotes the growth of the cells. Therefore, a higher cell proliferation is expected on the glass surface when compared to the metal surface.

The morphology was also checked by scanning electron microscopy (FEG-ESEM). As it can be seen in Fig. 8, the cell on the BG coating is spread in a multidirectional manner promoting contact between cells and the surface of the coating, as
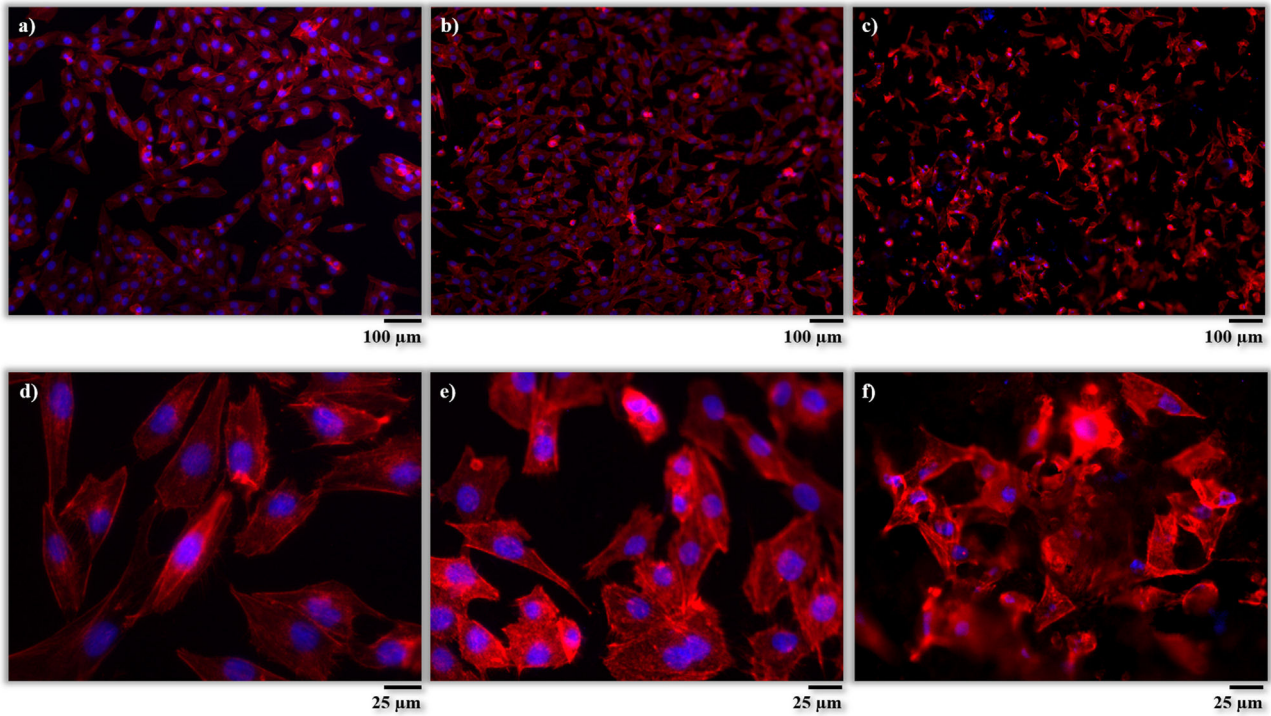
Fig. 7 – **Fluorescent micrographs of MG-63 cells after phalloidin-staining in direct contact with the different surfaces. (a) and (d) well-plate without sample, (b) and (e) AISI type 304 stainless steel, (c) and (f) BGC25 coating.**
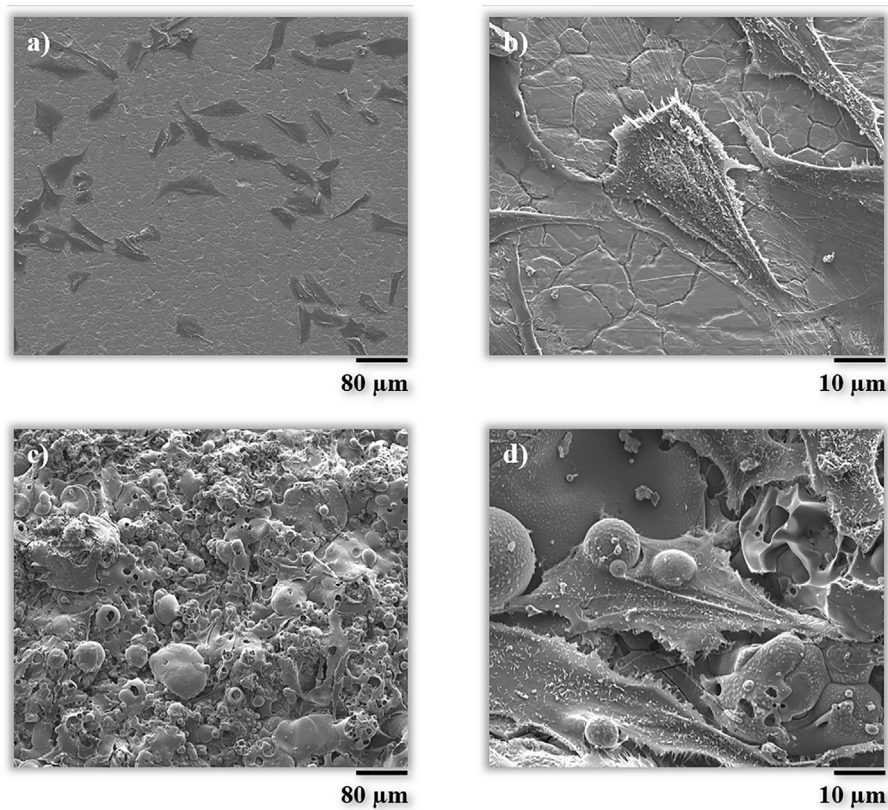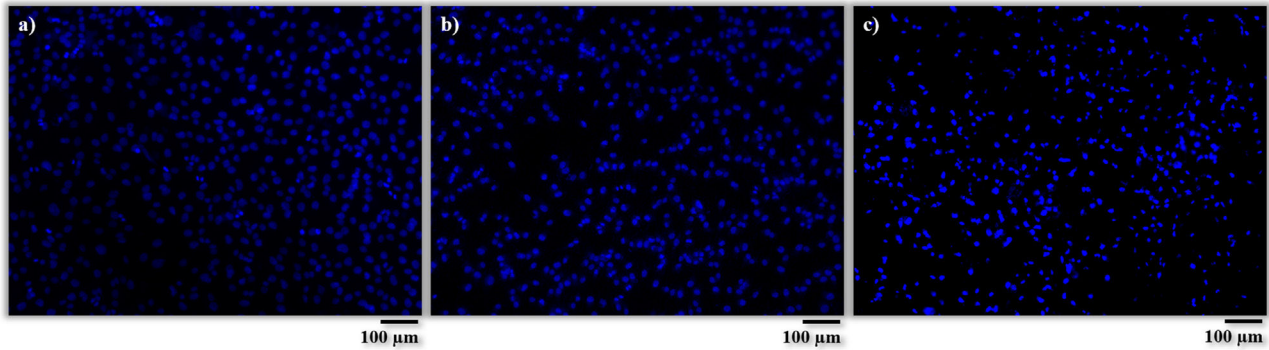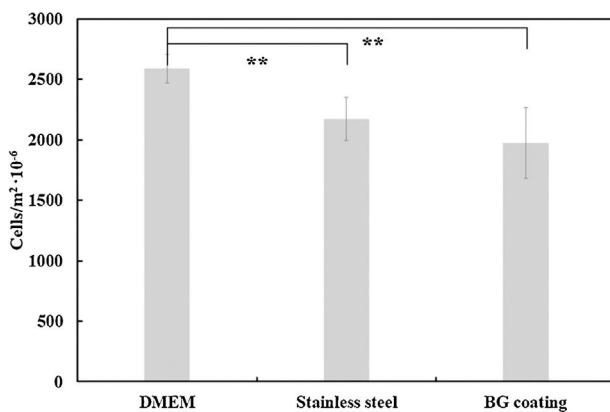

Fig. 8 – **FEG-ESEM micrographs of MG-63 cells on the tested surfaces (a) and (b) AISI type 304 stainless steel, (c) and (d) BGC25 coating after 1 day of cultivation.**

Fig. 9 – Fluorescent micrographs of MG-63 cell nucleus after Vybrant-staining in direct contact with the different surfaces (a) well-plate without sample, (b) AISI type 304 stainless steel, (c) BGC25 coating.

Fig. 10 – MG-63 cell amount (cells/m^2) on the well-plate, uncoated substrate and the bioactive glass coated substrate. Results expressed as mean with standard deviation. Statistically significant differences ($p < 0.01$) between means expressed with **.

discussed above. Splat-structured morphology of the BG coating promotes the growth of cells and hence their attachment, in comparison with a non-structured (smooth) and impervious surface, as in the case of the metallic substrate [48,49].

Regarding the number of cells, these results were quantitatively corroborated from micrographs obtained after Vybrant-staining (Fig. 9) and are shown in Fig. 10. There is a large number of cells in contact with all the materials tested. In addition, it can also be observed that there are no significant differences between the amount of cells (cells/m^2) on the AISI type 304 stainless steel substrate and the BGC25 coating.

In summary, it can be concluded that there is a strong interaction between the tested surfaces and MG-63 osteoblasts-like cells, due to the high amount of living cells present on each surface after 24 h of incubation. Despite not finding significant differences in the number of cells/m^2 on each surface (AISI type 304 stainless steel substrate and the BGC25 coating), the BG coating presents multidirectional growth of the cells, which promotes contact between cells and the surface. Moreover, a higher proliferation rate of cells on the surface of the bioactive glass coating can be expected compared to that

of the metal, as the surface roughness of the BGC25 coating and its open porosity are expected to promote ion exchange between the surface and the medium, which should positively affect cell behavior [48]. However, in order to corroborate this statement, prolonged incubation times with primary human osteoblast cells should be applied to appreciate how evolve both coated and uncoated samples.

Conclusions

This research addressed a complete in vitro study (immersion in SBF and cell culture) of a BG coating obtained by atmospheric plasma spraying technique. The following conclusions were inferred from the research:

– Both coatings (BGC25 and BGC38) exhibited a microstructure composed of partially deformed splats plenty of rounded pores and considerable thickness. As previously reported, this microstructure evolves from glassy-nature feedstocks which rapidly sinter and cool during plasma spraying. The amorphous nature of the feedstock was preserved after deposition. High porosity of the coatings was observed, which can enhance its bioactivity.
– Simulated body fluid test allowed to assess the precellular bioactivity of the coating. Bioactivity (formation of HCA) was monitored and verified by FTIR, FEG-ESEM, XRD and EDX and compared with that of the starting feedstock powder. All these tests confirmed the formation of the hydroxyapatite layer in the coating. However, the development rate of the HCA layer is slower on the coating surface than on the powder surface, due to the difference in the specific surface area.
– Surface characteristics of the coating consisting of deformed splats and high roughness resulted in good interaction between coating surface and human osteoblasts-like cells. Despite the similar number of cells/m^2 on the BG coated and uncoated surfaces, multidirectional growth of cells were observed on the BG surface leading to a potentially superior biological response of the coating. With the aim to corroborate this statement, longer incubation times will be performed.

Conflict of interests

The authors declare that they have no known competing financial interests or personal relationships that could have appeared to influence the work reported in this paper.

Acknowledgements

Appendix A. Supplementary data

Supplementary data associated with this article can be found, in the online version, at doi:10.1016/j.bsecv.2020.06.004.

REFERENCES

[1] J.R. Jones, A.G. Clare, Bio-glasses: An Introduction, 1st ed., John Wiley & Sons, Great Britain, 2012.

[2] T.M. Lee, E. Chang, B.C. Wang, C.Y. Yang, Characteristics of plasma-sprayed bioactive glass coatings on Ti–6A1–4V alloy: an in vitro study, Surf. Coat. Technol. 79 (1996) 170–177, http://dx.doi.org/10.1016/0257-8972(95)02463-8.

[3] T. Kitsugi, T. Nakamura, M. Oka, Y. Senaha, T. Goto, T. Shibuya, Bone-bonding behavior of plasma-sprayed coatings of Bioglass®, AW-glass ceramic, and tricalcium phosphate on titanium alloy, J. Biomed. Mater. Res. 30 (1996) 261–269, http://dx.doi.org/10.1002/(SICI)1097-4636(199602)30:2<261::AID-JBM17>3.0.CO;2-P.

[4] J.R. Jones, Review of bioactive glass: from Hench to hybrids, Acta Biomater. 23 (2015) 53–82, http://dx.doi.org/10.1016/j.actbio.2015.07.019.

[5] A.R. Boccaccini, M. Erol, W.J. Stark, D. Mohn, Z. Hong, J.F. Mano, Polymer/bioactive glass nanocomposites for biomedical applications: a review, Compos. Sci. Technol. 70 (2010) 1764–1776, http://dx.doi.org/10.1016/j.compscitech.2010.06.002.

[6] V. Cannillo, A. Sola, Potassium-based composition for a bioactive glass, Ceram. Int. 35 (2009) 3389–3393, http://dx.doi.org/10.1016/j.ceramint.2009.06.011.

[7] A. Sola, D. Bellucci, V. Cannillo, A. Cattini, Bioactive glass coatings: a review, Surf. Eng. 27 (2011) 560–572, http://dx.doi.org/10.1179/1743294410Y.0000000008.

[8] F. Baino, E. Verne, Glass-based coatings on biomedical implants: a state-of-the-art review, Biomed. Glasses 3 (2017) 1–17, http://dx.doi.org/10.1515/bglass-2017-0001.

[9] A. Al-Noaman, S.C.F. Rawlinson, R.G. Hill, The role of MgO on thermal properties, structure and bioactivity of bioactive glass coating for dental implants, J. Non-Cryst. Sol. 358 (2012) 3019–3027, http://dx.doi.org/10.1016/j.jnoncrysol.2012.07.039.

[10] E. Cañas, M. Vicent, E. Bannier, P. Carpio, M.J. Orts, E. Sánchez, Effect of particle size on processing of bioactive glass powder for atmospheric plasma spraying, J. Eur. Ceram. Soc. 36 (2016) 837–845, http://dx.doi.org/10.1016/j.jeurceramsoc.2015.09.039.

[11] A. Cattini, L. Latka, D. Bellucci, G. Bolelli, A. Sola, L. Lusvarghi, L. Pawlowski, V. Cannillo, Suspension plasma sprayed bioactive glass coatings: effects of processing on microstructure, mechanical properties and in-vitro behaviour, Surf. Coat. Technol. 220 (2013) 52–59, http://dx.doi.org/10.1016/j.surfcoat.2012.10.076.

[12] G. Bolelli, D. Bellucci, V. Cannillo, R. Gadow, A. Killinger, L. Lusvarghi, P. Müller, A. Sola, Comparison between suspension plasma sprayed and high velocity suspension flame sprayed bioactive coatings, Surf. Coat. Technol. 280 (2015) 232–249, http://dx.doi.org/10.1016/j.surfcoat.2015.08.039.

[13] S. Romeis, A. Hoppe, R. Detsch, A.R. Boccaccini, J. Schmidt, W. Peukert, Top-down processing of submicron 45S5 Bioglass® for enhanced in vitro bioactivity and biocompatibility, Proc. Eng. 102 (2015) 534–541, http://dx.doi.org/10.1016/j.proeng.2015.01.116.

[14] J. Henao, C.P. Salas, M. Monsalve, J.C. Castuera, O.B. Sanchez, Bio-active glass coatings manufactured by thermal spray: a status report, J. Mater. Res. Technol. 8 (2019) 4965–4984, http://dx.doi.org/10.1016/j.jmrt.2019.07.011.

[15] T. Bhatia, A. Ozturk, L. Xie, E.H. Jordan, B.M. Cetegen, M. Gell, X. Ma, N.P. Padture, Mechanisms of ceramic coating deposition in solution-precursor plasma spray, J. Mater. Res. 17 (2002) 2363–2372, http://dx.doi.org/10.1557/JMR.2002.0346.

[16] L. Xie, X. Ma, A. Ozturk, E.H. Jordan, N.P. Padture, B.M. Cetegen, D.T. Xiao, M. Gell, Processing parameter effects on solution precursor plasma spray process spray patterns, Surf. Coat. Technol. 183 (2004) 51–61, http://dx.doi.org/10.1016/j.surfcoat.2003.09.071.

[17] A. Mejias, R.T. Candidato Jr., L. Pawłowski, D. Chicot, Mechanical properties by instrumented indentation of solution precursor plasma sprayed hydroxyapatite coatings: analysis of microstructural effect, Surf. Coat. Technol. 298 (2016) 93–102, http://dx.doi.org/10.1016/j.surfcoat.2016.04.028.

[18] E. Cañas, M.J. Orts, A.R. Boccaccini, E. Sánchez, Microstructural and in vitro characterization of 45S5 bioactive glass coatings deposited by solution precursor plasma spraying (SPPS), Surf. Coat. Technol. 371 (2019) 151–160, http://dx.doi.org/10.1016/j.surfcoat.2018.12.057.

[19] Y. Xiao, L. Song, X. Liu, Y. Huang, T. Huang, J. Chen, Y. Wu, F. Wu, Bioactive glass-ceramic coatings synthesized by the liquid precursor plasma spraying process, J. Therm. Spray Technol. 20 (2011) 560–568, http://dx.doi.org/10.1007/s11666-010-9594-9.

[20] X. Liu, C. Ding, Z. Wang, Apatite formed on the surface of plasma-sprayed wollastonite coating immersed in simulated body fluid, Biomaterials 22 (2001) 2007–2012, http://dx.doi.org/10.1016/S0142-9612(00)00386-0.

[21] M.P. Ferraz, F.J. Monteiro, J.D. Santos, CaO-P_2O_5 glass hydroxyapatite double-layer plasma-sprayed coating: in vitro bioactivity evaluation, J. Biomed. Mater. Res. 45 (1999) 376–383, http://dx.doi.org/10.1002/(SICI)1097-4636(19990615)45:4<376::AID-JBM13>3.0.CO;2-S.

[22] C. Gabbi, A. Cacchioli, B. Locardi, E. Guadagnino, Bioactive glass coating: physicochemical aspects and biological findings, Biomaterials 16 (1995) 515–520.

[23] A. Oliva, A. Salerno, B. Locardi, V. Riccio, F. Della Ragione, P. Iardino, V. Zappia, Behaviour of human osteoblasts cultured on bioactive glass coatings, Biomaterials 19 (1998) 1019–1025, http://dx.doi.org/10.1016/S0142-9612(97)00249-4.

[24] C. Wu, Y. Ramaswamy, X. Liu, G. Wang, H. Zreigat, Plasma-sprayed $CaTiSiO_5$ ceramic coating on Ti–6Al–4V with excellent bonding strength, stability and cellular bioactivity, J.R. Soc. Interface 6 (2009) 159–168, http://dx.doi.org/10.1098/rsif.2008.0274.

[25] V. López, M. Vicent, E. Bannier, E. Cañas, A.R. Boccaccini, L. Cordero, E. Sánchez, 45S5 bioactive glass coatings by atmospheric plasma spraying obtained from feedstocks prepared by different routes, J. Mater. Sci. 49 (2014) 7933–7942, http://dx.doi.org/10.1007/s10853-014-8519-2.

[26] A.L.B. Maçon, T.B. Kim, E.M. Valliant, K. Goetschius, R.K. Brow, D.E. Day, A. Hoppe, A.R. Boccaccini, I.Y. Kim, C. Ohtsuki, T. Kokubo, A. Osaka, M. Vallet-Regí, D. Arcos, L. Fraile, A.J. Salinas, A.V. Teixeira, Y. Vueva, R.M. Almeida, M. Miola, C. Vitale-Brovarone, E. Verné, W. Höland, J.R. Jones, A unified in vitro evaluation for apatite-forming ability of bioactive glasses and their variants, J. Mater. Sci. Mater. Med. 26 (2015) 115–124, http://dx.doi.org/10.1007/s10856-015-5403-9.

[27] T. Kokubo, H. Takadama, How useful is SBF in predicting in vivo bone bioactivity? Biomaterials 27 (2006) 2907–2915, http://dx.doi.org/10.1016/j.biomaterials.2006.01.017.

[28] J.J. Blaker, J.E. Gough, V. Maquet, I. Notingher, A.R. Boccaccini, In vitro evaluation of novel bioactive composited based on bioglass®-filled polylactide foams for bone tissue engineering scaffolds, J. Biomed. Mater. Res. 67 (2003) 1401–1411, http://dx.doi.org/10.1016/j.biomaterials.2006.01.017.

[29] C. Vitale-Brobarone, E. Verné, L. Robiglio, P. Appendino, F. Bassi, G. Martinasso, G. Muzio, R. Canuto, Development of glass-ceramic scaffolds for bone tissue engineering: characterisation, proliferation of human osteoblasts and nodule formation, Acta Biomater. 3 (2007) 199–208, http://dx.doi.org/10.1016/j.actbio.2006.07.012.

[30] J. Ureña, S. Tsipas, A. Jimémez-Morales, E. Gordo, R. Detsch, A.R. Boccaccini, In-vitro study of the bioactivity and cytotoxicity response of Ti surfaces modified by Nb and Mo diffusion treatments, Surf. Coat. Technol. 335 (2018) 148–158, http://dx.doi.org/10.1016/j.surfcoat.2017.12.009.

[31] V. Canillo, A. Sola, Different approaches to produce coatings with bioactive glasses: enamelling vs plasma spraying, J. Eur. Ceram. Soc. 30 (2010) 2031–2039, http://dx.doi.org/10.1016/j.jeurceramsoc.2010.04.021.

[32] M. Takemotoa, S. Fujibayashia, M. Neoa, J. Suzukib, T. Kokuboc, T. Nakamura, Mechanical properties and osteoconductivity of porous bioactive titanium, Biomaterials 26 (2005) 6014–6023, http://dx.doi.org/10.1016/j.biomaterials.2005.03.019.

[33] K. Rezwan, Q.Z. Chen, J.J. Blaker, A.R. Boccaccini, Biodegradable and bioactive porous polymer/inorganic composite scaffolds for bone tissue engineering, Biomaterials 27 (2006) 3413–3431, http://dx.doi.org/10.1016/j.biomaterials.2006.01.039.

[34] L. Pawlowski, The science and engineering of thermal spray coatings, 2nd ed., John Wiley and Sons, Great Britain, 2008.

[35] J.R. Davis, Handbook of thermal spray technology, 1st ed., ASM International The USA, 2004.

[36] J.M. Gomez-Vega, E. Saiz, A.P. Tomsia, Glass-based coatings for titanium implant alloys, J. Biomed. Mater. Res. 46 (1999) 549–559, http://dx.doi.org/10.1002/(SICI)1097-4636(19990915)46:4<549::AID-JBM13>3.0.CO;2-M.

[37] A. Pazo, E. Saiz, A.P. Tomsia, Silicate glass coatings on Ti-based implants, Acta Mater. 46 (1998) 2551–2558, http://dx.doi.org/10.1016/S1359-6454(98)80039-6.

[38] G. Goller, The effect of bond coat on mechanical properties of plasma sprayed bioglass-titanium coatings, Ceram. Int. 30 (2004) 351–355, http://dx.doi.org/10.1016/S0272-8842(03)00107-X.

[39] M. Monsalve, H. Ageorges, E. Lopez, F. Vargas, F. Bolivar, Bioactivity and mechanical properties of plasma-sprayed coatings of bioglass powders, Surf. Coat. Technol. 220 (2013) 60–66, http://dx.doi.org/10.1016/j.surfcoat.2012.11.075.

[40] G.M. Nelson, J.A. Nychka, A.G. McDonald, Flame spray deposition of titanium alloy-bioactive glass composite coatings, J. Therm. Spray Tech. 20 (2011) 1339–1351, http://dx.doi.org/10.1007/s11666-011-9674-5.

[41] O.P. Filho, G.P. La Torre, L.L. Hench, Effect of crystallization on apatite-layer formation of bioactive glass 45S5, J. Biomed. Mater. Res. B 30 (1996) 509–514, http://dx.doi.org/10.1002/(SICI)1097-4636(199604)30:4<509::AID-JBM9>3.0.CO;2-T.

[42] A.A. El-Kheshen, F.A. Khaliafa, E.A. Saad, R.L. Elwan, Effect of Al_2O_3 addition on bioactivity, thermal and mechanical properties of some bioactive glasses, Ceram. Int. 34 (2008) 1667–1673, http://dx.doi.org/10.1016/j.ceramint.2007.05.016.

[43] M. Mačković, A. Hoppe, R. Detsch, D. Mohn, W.J. Stark, E. Spiecker, A.R. Boccaccini, Bioactive glass (type 45S5) nanoparticles: in vitro reactivity on nanoscale and biocompatibility, J. Nanopart. Res. 14 (2012) 966, http://dx.doi.org/10.1007/s11051-012-0966-6.

[44] S. Paul, A. Cipitria, I.O. Golosnoy, L. Xie, M.R. Dorfman, T.W. Clyne, Effects of impurity content on the sintering characteristics of plasma-sprayed zirconia, J. Therm. Spray Technol. 16 (2007) 798–803, http://dx.doi.org/10.1007/s11666-007-9097-5.

[45] S. Paul, A. Cipitria, S.A. Tsipas, T.W. Clyne, Sintering characteristics of plasma sprayed zirconia coatings containing different stabilisers, Surf. Coat. Technol. 203 (2009) 1069–1074, http://dx.doi.org/10.1016/j.surfcoat.2008.09.037.

[46] H. Pirayesh, J.A. Nychka, Sol–gel synthesis of bioactive glass-ceramic 45S5 and its in vitro dissolution and mineralization behavior, J. Am. Ceram. Soc. 96 (2013) 1643–1650, http://dx.doi.org/10.1111/jace.12190.

[47] M. Cerruti, D. Greenspan, K. Powers, Effect of pH and ionic strength on the reactivity of Bioglass® 45S5, Biomaterials 26 (2005) 1665–1674, http://dx.doi.org/10.1016/j.biomaterials.2004.07.009.

[48] A. Itälä, H.O. Ylänen, J. Yrjans, T. Heino, T. Hentunen, M.H.T. Hupa, Aro1, characterization of microrough bioactive glass surface: surface reactions and osteoblast responses in vitro, J. Biomed. Mater. Res 62 (2002) 404–411, http://dx.doi.org/10.1002/jbm.10273.

[49] R. Detsch, O. Guillon, L. Wondraczek, A.R. Boccaccini, Initial attatchment of rMSC and MG-63 cells on patterned bioglass® substrates, Adv. Eng. Mater. 14 (2012) B38–B44, http://dx.doi.org/10.1002/adem.201180068.